

Reaction chemistry, NMR spectroscopy, and X-ray crystallography of $[\text{Fe}_2(\mu\text{-SiMe}_2)_2(\text{CO})_4]$ and $[\text{Fe}_2(\mu\text{-SiMeCl})_2(\text{CO})_4]$. Electronic structure and bonding in Fe_2E_2 rings of $[\text{Fe}_2(\mu\text{-ER}_2)_2(\text{CO})_4]$ binuclear complexes (E = C, Si, Ge, Sn, Pb)

Richard S. Simons^a, Kevin J. Galat^a, John D. Bradshaw^a, Wiley J. Youngs^a,
Claire A. Tessier^{a,*}, Gabriel Aullón^b, Santiago Alvarez^b

^a Department of Chemistry, The University of Akron, 190 E Buchtel Commons, 111 KNCL, Akron, OH 44325-3601, USA

^b Departament de Química Inorgànica and Centre de Recerca en Química Teòrica (CeRQT), Universitat de Barcelona, Diagonal 647, 08028 Barcelona, Spain

Received 24 December 2000; accepted 19 March 2001

Abstract

The rings $[\text{Fe}_2(\mu\text{-SiRR}')_2(\text{CO})_8]$ (R = Me, R' = Me or Cl) react with HMPA to give the base-stabilized silylenes $[\text{Fe}(\text{-SiRR}'(\text{HMPA}))(\text{CO})_4]$. The reactions of $[\text{Fe}_2(\mu\text{-SiMe}_2)_2(\text{CO})_8]$ with DABCO, THF and PMe_3 have also been examined. The crystal structures of both $[\text{Fe}_2(\mu\text{-SiMe}_2)_2(\text{CO})_8]$ and $[\text{Fe}_2(\mu\text{-SiMeCl})_2(\text{CO})_8]$ show planar rings, C–H \cdots O=C short contacts and relatively short but non-bonding Si–Si distances. The possibility of through-ring M–M or E–E bonding in complexes of the type $[\text{M}_2(\mu\text{-ER}_2)_2(\text{CO})_8]$ (M is a transition metal and E is a Group 14 element) is analyzed with the help of theoretical calculations based on density functional theory. For compounds with 20 ring electrons (or a framework electron count, FEC, of eight), regular M_2E_2 rings are expected, with no short through-ring distances. The framework electron counting rules, geometry optimization of several model complexes and a structural database analysis consistently indicate that through-ring bonding exists only when the FEC is less than eight. In that case, the isomer with a short metal–metal bond is found to be significantly more stable than that with a short E–E distance. © 2001 Elsevier Science B.V. All rights reserved.

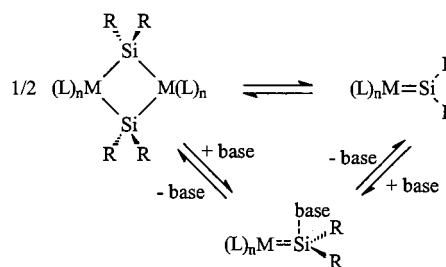
Keywords: Iron-silicon; Four-membered rings; Base-stabilized metal-silylenes; Weak hydrogen bonds; DFT calculations

1. Introduction

Metal–silicon four-membered rings occupy a peculiar niche in metal–silicon chemistry [1,2]. Their four-coordinate geometry at the silicon atom would suggest they are examples of normal-valent silicon yet the high positive ^{29}Si -NMR chemical shifts of many such rings would suggest that they should be considered as forms of low-valent silicon.

Equilibria have been proposed in which metal–silicon four-membered rings can be converted into more

conventional forms of low-valent silicon such as metal–silylenes or their base-stabilized complexes (Scheme 1) [3]. Cleavage of a metal–silicon ring by a base can give a base-stabilized silylene. With iron–silicon rings, such cleavage reactions were demonstrated for the complexes



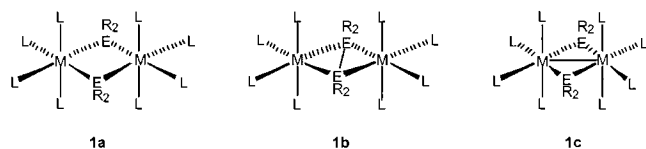
Scheme 1.

* Corresponding author. Fax: +1-330-972-7370.

E-mail address: tessier@chemistry.uakron.edu (C.A. Tessier).

$[\text{Fe}_2(\text{cyclo-}\mu\text{-SiF}_2\text{C}(t\text{-Bu)=CHSiF}_2)_2(\text{Cp})_2(\text{CO})_2]$ and $[\text{Fe}_2(\mu\text{-SiPh}_2)_2(\text{CO})_8]$ [4,5]. It has been claimed that the reverse process is exemplified by the formation of $[\text{Fe}_2(\mu\text{-SiMe}_2)_2(\text{CO})_8]$ upon heating the base-stabilized silylene complex $[\text{Fe}(\text{SiMe}_2(\text{HMPA}))(\text{CO})_4]$ [6]. In the interconversions between the rings and the base-stabilized silylene complexes it is not clear whether the free silylene is formed as an intermediate and in no case has a free iron–silylene been isolated from the equilibria in Scheme 1. However, good evidence for the involvement of iron–silylenes has been presented in the isomerization reactions of three-membered Fe_2Si rings [5a,7].

The double-bridged binuclear complexes of type $[\text{L}_4\text{M}(\mu\text{-ER}_2)_2\text{ML}_4]$, where M is a transition metal with approximately octahedral coordination geometry and E is a Group 14 element, present molecular structures that differ in the bonding within the M_2E_2 framework [8]. We can classify those structures into three families: those with *regular* M_2E_2 rings having no short through-ring distances (**1a**), those presenting short M–M distance (**1c**), and those with short E–E distance (**1b**). The existence of bonding between antipodal atoms in binuclear complexes obeys the framework electron counting rules [8,9]. In essence, the framework electron count (FEC) is the number of electrons contributed by the M and E atoms to the σ bonding of the M_2E_2 ring. Whenever the FEC is eight, a regular ring should be expected, whereas for molecules with less framework electrons (i.e. $\text{FEC} = 6$ or 4) a short through-ring distance is predicted. The main problem in determining the FEC stems from the fact that the transition metal atoms may store a variable number of electrons in non-bonding d orbitals, and it is not always straightforward to decide the number of framework electrons for a particular complex beforehand. It is usually simpler to determine the number of ring electrons (NRE) that includes those involved in M–E bonding, together with the metal d-electrons. For those complexes with octahedrally coordinated metal atoms, we have recently shown through a theoretical study combined with a structural database analysis that the FEC can effectively be considered as eight in such complexes when $\text{NRE} = 20$, whereas compounds with 18 or less ring electrons can be considered to have all six framework electrons ($\text{FEC} = 6$) [8].



In related complexes with square-planar Pt atoms, short through-ring Si··Si distances (~ 2.6 Å) [10] are considered indicative of a bonding interaction [9b,11]. For the iron rings reported here, $[\text{Fe}_2(\mu\text{-SiMe}_2)_2(\text{CO})_8]$ and $[\text{Fe}_2(\mu\text{-SiMeCl})_2(\text{CO})_8]$, it is not clear whether the

Si··Si distances of about 2.85 Å (see below) correspond to a bonding or non-bonding situation. Simple electron counting tells that for these complexes $\text{NRE} = 20$ (and $\text{FEC} = 8$). The FEC rules thus predict regular rings with no through-ring bonding interaction.

Herein we describe our explorations of the equilibria in Scheme 1 for the rings $[\text{Fe}_2(\mu\text{-SiMe}_2)_2(\text{CO})_8]$ and $[\text{Fe}_2(\mu\text{-SiMeCl})_2(\text{CO})_8]$. We report spectral characterization and X-ray crystal structure studies of these rings and several reaction products. To further substantiate the qualitative electron counting rules, we report a DFT theoretical study of $[\text{Fe}_2(\mu\text{-SiMe}_2)_2(\text{CO})_8]$ and $[\text{Fe}_2(\mu\text{-SiMeCl})_2(\text{CO})_8]$, their hypothetical oxidized derivatives (with $\text{NRE} = 18$), and several analogous compounds of the type $[\text{M}_2(\mu\text{-ER}_2)_2\text{L}_8]$, where M = Mn, Ru or Os; E = C, Si, Ge, Sn, or Pb.

2. Experimental

2.1. General procedures and materials

All manipulations were carried out in an argon or nitrogen atmosphere using standard Schlenk and glovebox techniques [12]. Hexane and toluene were distilled from a sodium/benzophenone ketyl. Methylene chloride was distilled from CaH_2 . All other chemicals were purchased from Aldrich or Petrarch and used without further purification. NMR spectra were obtained on 300 MHz instruments. Microanalytical determinations were performed at the Schwarzkopf Microanalytical Laboratory, Woodside, NY. Mass spectroscopy measurements were performed at the University of Nebraska, Mass Spectroscopy Laboratory.

2.2. Preparation of the iron–silyl hydrides $\text{FeH}(\text{CO})_4(\text{SiMe}_2\text{Cl})$ and $\text{FeH}(\text{CO})_4(\text{SiMeCl}_2)$

The iron–silyl hydrides were prepared according to the literature [13]. A medium pressure mercury lamp was substituted for a high-pressure mercury lamp and a Pyrex vessel was substituted for a quartz vessel.

2.3. Preparation of $[\text{Fe}_2(\mu\text{-SiMe}_2)_2(\text{CO})_8]$ and $[\text{Fe}_2(\mu\text{-SiMeCl})_2(\text{CO})_8]$

These complexes were prepared according to the literature preparation from $\text{FeH}(\text{CO})_4(\text{SiMe}_2\text{Cl})$ or $\text{FeH}(\text{CO})_4(\text{SiMeCl}_2)$, respectively [13]. $[\text{Fe}_2(\mu\text{-SiMe}_2)_2(\text{CO})_8]$: $^1\text{H-NMR}$ (C_6D_6 , 300 MHz): $\delta = 0.96$ (s, 6H); $^{13}\text{C-NMR}$ (C_6D_6 , 75 MHz): $\delta = 11.5$ (s, Me), 208.5, 205.7 (s, $\text{C}\equiv\text{O}$); $^{29}\text{Si-NMR}$ (C_6D_6 , 60 MHz): $\delta = 17.8$ (s), MS (EI, m/e): $\text{M}^+ - \text{CO}$ 424, $\text{M}^+ - n$ CO successive peaks 396, 368, 340, 312, 284, 256, 228. $[\text{Fe}_2(\mu\text{-SiMeCl})_2(\text{CO})_8]$: $^1\text{H-NMR}$ (300 MHz, C_6D_6): $\delta = 1.32, 1.48$ (s, 3H, *cis* and *trans*); $^{13}\text{C-NMR}$ (75

MHz, C_6D_6): $\delta = 17.4, 17.9$ (s, MeSi, *cis* and *trans*), 203.6, 206.8 (C=O *cis* to Si), 202.1, 205.2 (C=O *trans* to Si); ^{29}Si -NMR (60 MHz, C_6D_6): $\delta = 74.1$ (*cis*), 73.5 (*trans*).

2.4. Preparation of $[Fe(SiMe_2(HMPA))(CO)_4]$

HMPA (0.12 ml, 0.66 mmol) was added by syringe to a stirred solution of $[Fe_2(\mu-SiMe_2)_2(CO)_8]$ (0.15 g, 0.33 mmol) in 3 ml of C_6D_6 . Stirring was continued for 4 h. The reaction was monitored by 1H -NMR and determined to be complete. Slow addition of 0.5 ml hexane gave $[Fe(SiMe_2(HMPA))(CO)_4]$ as colorless crystals. 1H -NMR (300 MHz, C_6D_6): $\delta = 0.89$ (s, 6H), 2.17 (d, 18H, $J_{PH} = 12.4$ Hz); ^{13}C -NMR (75 MHz, C_6D_6): $\delta = 10.96$ (s, Me₂Si), 36.37 (d, NMe₂, $J_{PC} = 4.9$ Hz), 218.86 (s, C=O); ^{31}P -NMR (121 MHz, C_6D_6): $\delta = 24.08$ (s); ^{29}Si -NMR (60 MHz, C_6D_6): $\delta = 91.8$ (d, $J_{PSi} = 23.4$ Hz).

2.5. Preparation of $[Fe(SiMeCl(HMPA))(CO)_4]$

HMPA (1.38 ml, 8.0 mmol) was added by syringe to a stirred solution of $[Fe_2(\mu-SiMeCl)_2(CO)_8]$ (1.7 g, 3.4 mmol) in 30 ml of toluene. Stirring was continued for 4 h. Slow addition of 20 ml hexane gave $[Fe(SiMeCl(HMPA))(CO)_4]$ as the solvated $[Fe(SiMeCl(HMPA))(CO)_4](toluene)_{10}$ (by 1H -NMR integration). The volatile components were slowly removed in vacuo to yield $[Fe(SiMeCl(HMPA))(CO)_4]$ as colorless crystals: Yield 1.46 g, 96.7%, 1H -NMR (300 MHz, C_6D_6): $\delta = 1.16$ (s, 3H), 2.17 (d, 18H, $J_{PH} = 10.5$ Hz); ^{13}C -NMR (75 MHz, C_6D_6): $\delta = 15.91$ (s, MeClSi), 36.69 (d, NMe, $J_{PC} = 4.9$ Hz), 217.42 (s, C=O); ^{29}Si -NMR (60 MHz, C_6D_6): $\delta = 90.16$ (d, $J_{PSi} = 28$ Hz).

2.6. Preparation of $[Fe(SiMe_2(DABCO))(CO)_4]$

$[Fe_2(\mu-SiMe_2)_2(CO)_8]$ (0.1 g, 0.22 mmol) and DABCO (0.074 g, 0.44 mmol) were stirred in 3 ml of d^8 -toluene. 1H -NMR showed the reaction to progress over 30 days to completeness. 1H -NMR (300 MHz, d^8 -toluene): $\delta = 0.48$ (s, 6H), 2.0 (t, 6H, $J = 7.25$ Hz), 2.28 (t, 6H, $J = 7.25$ Hz); ^{13}C -NMR (75 MHz, d^8 -toluene): $\delta = 6.4$ (s, SiMe) 45.1 (s, SiN(CH₂)), 46.7 (s, N(CH₂)), 217.9 (s, C=O); ^{29}Si (60 MHz, d^8 -toluene): $\delta = 115.9$ (s).

2.7. Reaction of $[Fe_2(\mu-SiMe_2)_2(CO)_8]$ with THF

$[Fe_2(\mu-SiMe_2)_2(CO)_8]$ (0.10 g, 0.22 mmol) was combined with THF (0.05 ml, 0.44 mmol) in 3 ml of C_7D_8 and stirred. The solution turned brown. After 10 days a fine gray precipitate formed. Reaction progress was monitored by 1H - and ^{29}Si -NMR and judged complete after 20 days (Section 3).

2.8. Reaction of $[Fe_2(\mu-SiMe_2)_2(CO)_8]$ with PMe_3

$[Fe_2(\mu-SiMe_2)_2(CO)_8]$ (0.10 g, 0.22 mmol) was dissolved in 30 ml of toluene. With stirring PMe_3 (0.050 ml, 0.44 mmol) was added via syringe. The solution turned from a green to an orange color immediately. The reaction was refluxed for 12 h under a stream of nitrogen. The volatile components were removed under vacuum leaving a yellow residue. The residue was dissolved in 10 ml of CH_2Cl_2 and 20 ml of hexane was added. Cooling to $-30^\circ C$ overnight yielded a white fluffy precipitate, which was filtered out. The 1H -NMR spectrum of the solid ($\delta = 0.30$ ppm (broad)) suggests it is a mixture of $(SiMe_2)_n$ oligomers [14]. The filtrate was reduced in volume to 5 ml. Long needle-like crystals of *trans*- $Fe(PMe_3)_2(CO)_3$ (0.059 g, 90%), suitable for X-ray diffraction, formed. Spectra for *trans*- $Fe(PMe_3)_2(CO)_3$ were identical to that reported in literature [15].

2.9. X-ray crystallography

All manipulations were performed on a Syntex P2₁ diffractometer with graphite monochromated Mo-K α ($\lambda = 0.70173$) radiation at $-144^\circ C$ for $[Fe_2(\mu-SiMeCl)_2(CO)_8]$ and $[Fe(SiMeCl(HMPA))(CO)_4]$, $18^\circ C$ for $[Fe_2(\mu-SiMe_2)_2(CO)_8]$ and $[Fe(SiMe_2(HMPA))(CO)_4]$ and 20° for $Fe(PMe_3)_2(CO)_3$. A crystal of each was sealed in glass capillaries under Ar. Unit cell parameters were obtained from the least square refinement of the indices and angles of 25 centered reflections with 2θ between 20 and 30° . All intensity data were corrected for Lorentz and polarization effects. An empirical absorption correction was performed utilizing the method of ψ -scans for $[Fe_2(\mu-SiMeCl)_2(CO)_8]$, $[Fe(SiMeCl(HMPA))(CO)_4]$, $Fe(PMe_3)_2(CO)_3$ and applied to the intensity data. The structures of $[Fe_2(\mu-SiMe_2)_2(CO)_8]$, $[Fe_2(\mu-SiMeCl)_2(CO)_8]$, and $[Fe(SiMeCl(HMPA))(CO)_4]$ were solved by direct methods and Fourier difference techniques and refined to convergence by a least squares refinement using anisotropic displacement parameters for all non-hydrogen atoms and isotropic displacement parameters for hydrogen atoms. The positions of the hydrogen atoms of $[Fe_2(\mu-SiMe_2)_2(CO)_8]$ and $[Fe_2(\mu-SiMeCl)_2(CO)_8]$ were found but they did not refine satisfactorily. Hydrogen atoms were placed in idealized positions that were close to the found positions. The methyl and chloro groups of $[Fe(SiMeCl(HMPA))(CO)_4]$ were disordered with a 67:33 ratio (%) of one hand to the other. One of the carbonyl oxygen atoms (O(4)) of $[Fe(SiMeCl(HMPA))(CO)_4]$ was also disordered. Crystal data, data collection and data reduction for $[Fe_2(\mu-SiMe_2)_2(CO)_8]$, $[Fe_2(\mu-SiMeCl)_2(CO)_8]$ and $[Fe(SiMeCl(HMPA))(CO)_4]$ are listed in Table 1.

Table 1

Crystal data, data collection and reduction, and refinement details for $[\text{Fe}(\text{CO})_4(\text{SiMe}_2)]_2$, $[\text{Fe}(\text{CO})_4(\text{SiMeCl})]_2$ and $\text{Fe}(\text{CO})_4(\text{SiMeCl}(\text{HMPA}))$

Compound	$[\text{Fe}_2(\text{SiMe}_2)_2(\text{CO})_8]$	$[\text{Fe}_2(\text{SiMeCl})_2(\text{CO})_8]$	$[\text{Fe}(\text{SiMeCl}(\text{HMPA}))(\text{CO})_4]$
Empirical formula	$\text{C}_{12}\text{H}_{12}\text{Fe}_2\text{O}_8\text{Si}_2$	$\text{C}_{10}\text{H}_6\text{Cl}_2\text{Fe}_2\text{O}_8\text{Si}_2$	$\text{C}_{11}\text{H}_{21}\text{ClFePN}_3\text{O}_5\text{Si}$
Formula weight	452.1	492.93	425.67
Crystal system	Monoclinic	Monoclinic	Monoclinic
Space group	$P2_1/c$	$P2_1/n$	$P2_1/n$
Unit cell dimensions			
a (Å)	14.662(7)	8.607(2)	8.481(2)
b (Å)	9.516(4)	11.311(2)	15.805(3)
c (Å)	14.000(7)	9.123(2)	29.748(6)
α (°)	90.0	90.0	90.0
β (°)	105.28(4)	97.87(3)	91.21(3)
γ (°)	90.0	90.0	90.0
V (Å ³)	1884.4(15)	879.8(3)	3986.6(15)
Z	4	2	8
D_{calc} (Mg m ⁻³)	1.594	1.861	1.418
μ (Mo–K α) (mm ⁻¹)	1.699	2.122	1.053
Crystal size (mm)	$0.2 \times 0.2 \times 0.2$	$0.2 \times 0.2 \times 0.2$	$0.3 \times 0.3 \times 0.2$
Scan type	$2\theta-\theta$	ω	$2\theta-\theta$
Scan range (°)	2.00	1.60	2.00
2θ range (°)	3.0–45.0	3.5–55.0	3.5–45.0
Min, max transmissions	Not applied	0.5161/0.6005	0.2531/0.2924
No. of unique data	2447	1768	5493
Independent reflections F^2	1811	1135	5128
No. of parameters	221	110	479
Goodness-of-fit	1.000	1.023	1.012
R (%)	7.94	5.21	3.29
wR_2 (%)	19.64	12.37	7.99

The structures of $[\text{Fe}(\text{SiMe}_2(\text{HMPA}))(\text{CO})_4]$ and $\text{Fe}(\text{PMe}_3)_2(\text{CO})_3$ were solved by direct methods and Fourier difference techniques and refined to convergence by a least squares refinement using anisotropic displacement parameters for the iron, phosphorus, silicon and oxygen atoms and isotropic displacement parameters for all carbon and hydrogen atoms. The crystal structure of $[\text{Fe}(\text{SiMe}_2(\text{HMPA}))(\text{CO})_4]$ had already been published [6] and, therefore, it is not included in Table 1. The non-hydrogen atoms in the structure of $\text{Fe}(\text{PMe}_3)_2(\text{CO})_3$ were clearly located, however, structure solution had a high R -value. Because we obtained the structure of $\text{Fe}(\text{PMe}_3)_2(\text{CO})_3$ only to verify its presence, it will not be discussed further.

2.10. Computational details

Density functional calculations were performed with the Gaussian 94 suite of programs [16]. The hybrid B3LYP-DFT method was applied, in which the Becke three parameters exchange functional [17] and the Lee–Yang–Parr correlation functional were used [18]. The double- ζ basis set for the valence and outermost core orbitals combined with pseudopotentials known as LANL2DZ were used for all the atoms [19]. The geometries were fully optimized using gradient techniques with the only restriction of assuming D_{2h} symmetry for the $\text{Fe}_2\text{Si}_2(\text{CO})_8$ core.

2.11. Structural database search

The structural data was obtained through a systematic search in the *Cambridge Structural Database* [20] (version 5.18) for compounds of general formula $[(L_4M)_2(\mu\text{-ER}_2)_2]$. The search allowed for compounds with M_2E_2 cores, M being any transition metal and E a Group 14 element. For Fig. 6 a search of all *cis*- $\text{Fe}(\text{CO})_4L_2$ fragments was carried out, imposing the requirements that the structures were not disordered, the refinement had an R factor of 0.05 or less, and there were no direct L–L bonds.

3. Results and discussion

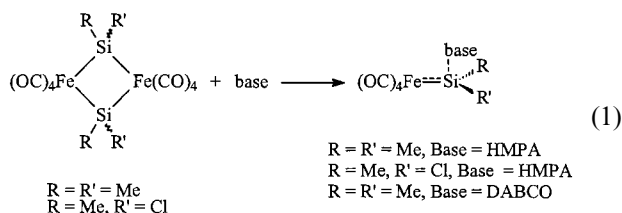
3.1. Synthesis and reaction chemistry

The complexes $[\text{Fe}_2(\mu\text{-SiMe}_2)_2(\text{CO})_8]$ and $[\text{Fe}_2(\mu\text{-SiMeCl})_2(\text{CO})_8]$ were isolated by the previously reported synthesis involving the reaction of AlCl_3 with $[\text{Et}_4\text{N}][\text{Fe}(\text{SiMe}_2\text{Cl})(\text{CO})_4]$ or $[\text{Et}_4\text{N}][\text{Fe}(\text{SiMeCl}_2)(\text{CO})_4]$, respectively, in hexane [13]. Low yields of the rings are obtained because the two starting materials have low solubility in hexane. Attempts to improve the yields by using aromatic solvents or using the more soluble AlBr_3 instead of AlCl_3 were unsuccessful.

The potential for *cis* and *trans* isomers (relative to the ring plane) exists for the ring $[\text{Fe}_2(\mu\text{-SiMeCl})_2(\text{CO})_8]$. The crystal structure (see below) shows exclusively the *trans* isomer and only one type of crystal was observed. In contrast, in solution both isomers were observed by NMR spectroscopy (see below).

The rings are colorless and are air and moisture sensitive. Solutions of $[\text{Fe}_2(\mu\text{-SiMe}_2)_2(\text{CO})_8]$ and $[\text{Fe}_2(\mu\text{-SiMeCl})_2(\text{CO})_8]$ are not stable for long periods even in the absence of oxygen and water. Solutions are both thermally and light sensitive giving red impurities. The photochemical conversion of $[\text{Fe}_2(\mu\text{-SiMeR})_2(\text{CO})_8]$ (R = Me or Cl) to $[\text{Fe}_2(\text{CO})_6(\mu\text{-CO})(\mu\text{-SiMeR})_2]$ has been reported [13]. Rings of type $[\text{Fe}_2(\mu\text{-SiRR}')_2(\text{CO})_8]$ appear to be unstable irrespective of the substituents on silicon. $[\text{Fe}(\text{CO})_4(\mu\text{-SiPh}_2)]_2$ is thermally unstable and gives a compound with a bridging carbonyl, presumably $[\text{Fe}_2(\mu\text{-SiPh}_2)_2(\mu\text{-CO})(\text{CO})_6]$, upon heating [21]. Three examples of $[\text{Fe}_2(\mu\text{-SiRR}')_2(\text{CO})_8]$ (SiRR' = SiPhMe; SiPhH; and 1-silaphenenediyl) appear to be too unstable to be isolated because only the $[\text{Fe}_2(\mu\text{-SiRR}')_2(\mu\text{-CO})(\text{CO})_6]$ rings are isolated instead [21,22]. These observations do not support the claim that the thermal decomposition of $[\text{Fe}(\text{SiMe}_2(\text{HMPA}))(\text{CO})_4]$ at 110° gives $[\text{Fe}_2(\mu\text{-SiMe}_2)_2(\text{CO})_8]$ [6]. As will be discussed below, we believe that $[\text{Fe}_2(\mu\text{-SiMe}_2)_2(\mu\text{-CO})(\text{CO})_6]$ was probably isolated instead.

The reactions of $[\text{Fe}_2(\mu\text{-SiMe}_2)_2(\text{CO})_8]$ and $[\text{Fe}_2(\mu\text{-SiMeCl})_2(\text{CO})_8]$ with Lewis bases were investigated. $[\text{Fe}_2(\mu\text{-SiMe}_2)_2(\text{CO})_8]$ and $[\text{Fe}_2(\mu\text{-SiMeCl})_2(\text{CO})_8]$ reacted smoothly with hexamethylphosphoramide (HMPA) to yield the base-stabilized iron–silylene complexes $[\text{Fe}(\text{SiMe}_2(\text{HMPA}))(\text{CO})_4]$ and $[\text{Fe}(\text{SiMeCl}(\text{HMPA}))(\text{CO})_4]$ (Eq.(1)). The reaction took place with



only a two-fold excess of HMPA at room temperature in C_6D_6 or $\text{CD}_3\text{C}_6\text{D}_5$ solution. The reaction of $[\text{Fe}_2(\mu\text{-SiMe}_2)_2(\text{CO})_8]$ with 1,4-diazobicyclo-2,2,2-octane (DABCO) to give $[\text{Fe}(\text{SiMe}_2(\text{DABCO}))(\text{CO})_4]$ is significantly slower than that with HMPA (~30 days versus 4 h), indicating that DABCO is less basic than HMPA to the silicon center. Only one of the two Lewis base sites of DABCO reacts, even when the reaction of DABCO and $[\text{Fe}_2(\mu\text{-SiMe}_2)_2(\text{CO})_8]$ is carried out in a 1:2 ratio.

Firm evidence for the formation of $[\text{Fe}(\text{SiMe}_2(\text{base}))(\text{CO})_4]$ from the reactions of $[\text{Fe}_2(\mu\text{-SiMe}_2)_2(\text{CO})_8]$ with the bases THF and PMe_3 was not obtained. A slow reaction between $[\text{Fe}_2(\mu\text{-SiMe}_2)_2(\text{CO})_8]$ and

THF took place in which $[\text{Fe}(\text{SiMe}_2(\text{THF}))(\text{CO})_4]$ may have formed as an intermediate (see below). Further reaction took place and the ultimate products could not be identified. It is interesting to note that the ring $[\text{Fe}_2(\mu\text{-SiMe}_2)_2(\text{CO})_8]$ is more reactive to THF than the base-stabilized silylene $[\text{Fe}(\text{SiMe}_2(\text{HMPA}))(\text{CO})_4]$, which is prepared in and crystallized from THF [6]. The reaction of $[\text{Fe}_2(\mu\text{-SiMe}_2)_2(\text{CO})_8]$ with PMe_3 was fast and gave no evidence of $[\text{Fe}(\text{SiMe}_2(\text{PMe}_3))(\text{CO})_4]$ or $[\text{Fe}_2(\mu\text{-SiMe}_2)_2(\text{PMe}_3)_2(\text{CO})_6]$ intermediates. Formation of *trans*- $\text{Fe}(\text{CO})_3(\text{PMe}_3)_2$ (90%) and, presumably, a mixture of oligomers $(\text{SiMe}_2)_n$ was observed. The reaction of $[\text{Fe}(\text{SiMe}_2(\text{HMPA}))(\text{CO})_4]$ with PPh_3 yields *trans*- $\text{Fe}(\text{PPh}_3)_2(\text{CO})_3$, though, in this case, isolation of the intermediate carbonyl substituted product $[\text{Fe}(\text{SiMe}_2(\text{HMPA}))(\text{PPh}_3)(\text{CO})_3]$ was possible [6]. In contrast to the reaction of $[\text{Fe}_2(\mu\text{-SiMe}_2)_2(\text{CO})_8]$ with PMe_3 , substitution of a carbonyl ligand occurs in the reaction of $[\text{Fe}_2(\mu\text{-SiPh}_2)_2(\text{CO})_8]$ with PPh_3 and gives the ring $[\text{Fe}_2(\mu\text{-SiPh}_2)_2(\text{PPh}_3)_2(\text{CO})_6]$ [21b].

3.2. Spectral characterization

The previously reported rings $[\text{Fe}_2(\mu\text{-SiMe}_2)_2(\text{CO})_8]$ and $[\text{Fe}_2(\mu\text{-SiMeCl})_2(\text{CO})_8]$ had not been characterized by NMR spectroscopy. For $[\text{Fe}_2(\mu\text{-SiMe}_2)_2(\text{CO})_8]$, a singlet is observed in the ^1H - and ^{13}C -NMR spectra for the methyl substituents. Two resonances are observed in the ^{13}C -NMR at 205.7 and 206.8 ppm for the carbonyl substituents. This is consistent with an octahedral geometry at the iron center and the dimeric structure in solution. The ^1H - and the ^{13}C -NMR data for $[\text{Fe}_2(\mu\text{-SiMeCl})_2(\text{CO})_8]$ are similar to that of $[\text{Fe}_2(\mu\text{-SiMe}_2)_2(\text{CO})_8]$, however, both *cis* and *trans* isomers are present in solution. Integration of the ^1H -NMR for the methyl resonances of $[\text{Fe}_2(\mu\text{-SiMeCl})_2(\text{CO})_8]$ indicates that the isomers are present in a 1:2 ratio. Presumably, the more abundant isomer has the *trans* structure. The ^{29}Si -NMR spectrum of $[\text{Fe}_2(\mu\text{-SiMe}_2)_2(\text{CO})_8]$ shows a single resonance at 17.8 ppm whereas the spectrum of $[\text{Fe}_2(\mu\text{-SiMeCl})_2(\text{CO})_8]$ shows two resonances at 74.1 and 73.5 ppm for the *cis* and *trans* isomers, respectively. As expected [2], these chemical shifts are less positive than those in iron–silicon rings with iron–iron bonds. The ^{29}Si -NMR chemical shift for the product from the thermal decomposition of $[\text{Fe}(\text{SiMe}_2(\text{HMPA}))(\text{CO})_4]$ at 110° is 159 or 161 ppm. This downfield chemical shift has been assigned to $[\text{Fe}_2(\mu\text{-SiMe}_2)_2(\text{CO})_8]$ but we believe it is more consistent to assign it to iron–iron bonded $[\text{Fe}_2(\mu\text{-SiMe}_2)_2(\mu\text{-CO})(\text{CO})_6]$.

The parent ion was not observed in the mass spectrum of $[\text{Fe}_2(\mu\text{-SiMe}_2)_2(\text{CO})_8]$. Rather, peaks due to successive loss of the eight carbonyl ligands were observed. Such a fragmentation pattern is typical of carbonyl-containing metal–silicon compounds [23].

The formation of the base-stabilized adducts $[\text{Fe}(\text{SiMe}_2(\text{HMPA}))(\text{CO})_4]$, $[\text{Fe}(\text{SiMeCl}(\text{HMPA}))(\text{CO})_4]$, and $[\text{Fe}(\text{SiMe}_2(\text{DABCO}))(\text{CO})_4]$ from Eq.(1). is supported by NMR data. NMR spectral data for $[\text{Fe}(\text{SiMe}_2(\text{HMPA}))(\text{CO})_4]$ had been reported and are largely in agreement with the spectral parameters we observed [6]. Any minor discrepancies are probably due to low levels of magnetic iron impurities. These discrepancies initially were of concern and so the crystal structure of $[\text{Fe}(\text{SiMe}_2(\text{HMPA}))(\text{CO})_4]$ was obtained (see below). The three base-stabilized silylene complexes show singlets near 1 ppm in the ^1H -NMR spectra for the methyl groups. Each is shifted upfield from that of the corresponding ring. The three base-stabilized silylene complexes show a single resonance for the carbonyl ligands in the ^{13}C -NMR spectrum indicating a stereochemically non-rigid, trigonal bipyramidal geometry at the iron center. The ^{29}Si -NMR signals for $[\text{Fe}(\text{SiMe}_2(\text{HMPA}))(\text{CO})_4]$ and $[\text{Fe}(\text{SiMeCl}(\text{HMPA}))(\text{CO})_4]$

$(\text{CO})_4]$ are observed as doublets because of coupling with the phosphorus atom of the HMPA ligand at 91.8 ($J_{\text{Si-P}} = 24$ Hz) and 90.2 ppm ($J_{\text{Si-P}} = 28$ Hz), respectively. The ^{29}Si -NMR spectrum of $[\text{Fe}(\text{SiMe}_2(\text{DABCO}))(\text{CO})_4]$ exhibits a singlet at δ 115 ppm. These ^{29}Si -NMR chemical shifts are consistent with base-stabilized silylene complexes [3].

As shown by the ^{29}Si -NMR spectrum, the reaction of $[\text{Fe}_2(\mu\text{-SiMe}_2)_2(\text{CO})_8]$ with THF gave two silicon-containing products at 146 and -12 ppm. The former ^{29}Si chemical shift is consistent with a base-stabilized silylene complex [3]. The formation of an unidentified precipitate was also observed and, concurrently, NMR signals broadened, presumably due to ferromagnetic or paramagnetic iron products. A THF-stabilized iron silylene has been reported from the reaction of the ring $[\text{Fe}_2(\text{cyclo-}\mu\text{-SiF}_2\text{C}(t\text{-Bu})=\text{CHSiF}_2)_2(\text{Cp})_2(\text{CO})_2]$ and THF [4a].

3.3. X-ray crystallography

The thermal ellipsoid drawings for the single-crystal structures of $[\text{Fe}_2(\mu\text{-SiMe}_2)_2(\text{CO})_8]$ and $[\text{Fe}_2(\mu\text{-SiMeCl})_2(\text{CO})_8]$ are given in Figs. 1 and 2, respectively. The unit cell for $[\text{Fe}_2(\mu\text{-SiMe}_2)_2(\text{CO})_8]$ contains two independent molecules whose structural parameters are similar. Selected bond distances and angles for $[\text{Fe}_2(\mu\text{-SiMe}_2)_2(\text{CO})_8]$ and $[\text{Fe}_2(\mu\text{-SiMeCl})_2(\text{CO})_8]$ are listed in Table 2.

The structures of $[\text{Fe}_2(\mu\text{-SiMe}_2)_2(\text{CO})_8]$ and $[\text{Fe}_2(\mu\text{-SiMeCl})_2(\text{CO})_8]$ consist of planar iron–silicon rings. The Fe–Fe distances of about 3.85 and 3.78 Å for $[\text{Fe}_2(\mu\text{-SiMe}_2)_2(\text{CO})_8]$ and $[\text{Fe}_2(\mu\text{-SiMeCl})_2(\text{CO})_8]$, respectively, indicate there is no iron–iron bonding interaction across the rings. The cross-ring Si–Si distances are only about 0.2 Å longer than the longest known Si–Si bond (2.69 Å [24]) and are about 20% longer than the sum of two silicon covalent radii [25]. The two independent molecules of $[\text{Fe}_2(\mu\text{-SiMe}_2)_2(\text{CO})_8]$ have marginally different Fe–Si bond distances whereas the Fe–Si distances within each molecule are the same (2.400(3)–2.402(3) versus 2.412(3)–2.414(3) Å). Substitution of an alkyl substituent by chloride usually leads to a shorter metal–silicon distance [1]. Consistent with this general principle, the Fe–Si distance in $[\text{Fe}_2(\mu\text{-SiMeCl})_2(\text{CO})_8]$ (2.363(3) Å) is shorter than in $[\text{Fe}_2(\mu\text{-SiMe}_2)_2(\text{CO})_8]$. The Fe–Si distances in both rings are toward the longer end of the range of other Fe–Si bond distances (2.20–2.42 Å) [1a] and are similar to that calculated for the base-free silylene complex $[\text{Fe}(\text{SiH}_2)(\text{CO})_4]$ (2.41 Å) [26]. The Si–Fe–Si angles of the two rings are about 16–17° less than the 90° value expected for ideal octahedral geometry at iron. The Fe–Si–Fe angles for $[\text{Fe}_2(\mu\text{-SiMe}_2)_2(\text{CO})_8]$ and $[\text{Fe}_2(\mu\text{-SiMeCl})_2(\text{CO})_8]$ are only 3° smaller than the value expected for tetrahedral geometry whereas the C–Si–C angles are somewhat more compressed.

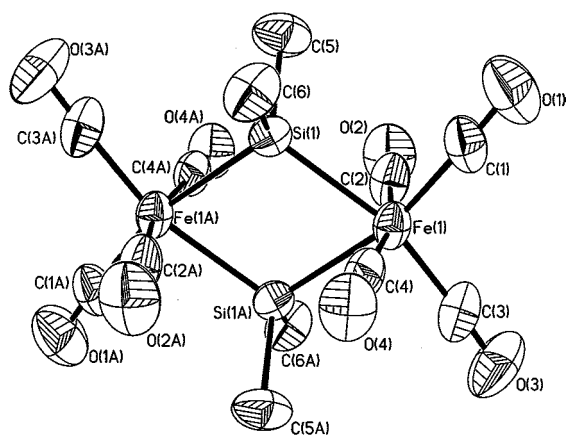


Fig. 1. Molecular structure of one of the two molecules of $[\text{Fe}(\text{CO})_4(\text{SiMe}_2)_2]$ with the thermal ellipsoids drawn at the 50% probability level. The hydrogen atoms have been omitted for clarity.

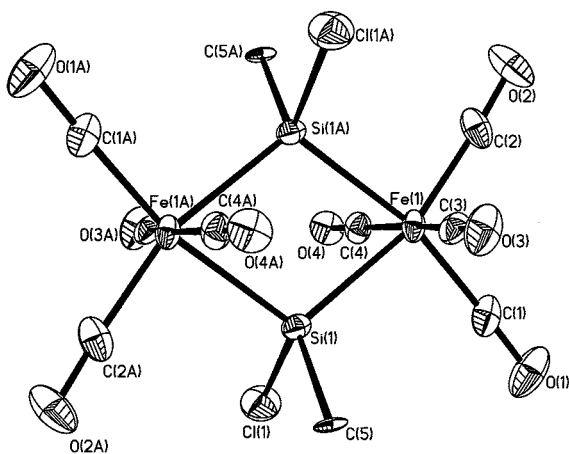


Fig. 2. Molecular structure of $[\text{Fe}_2(\mu\text{-SiMeCl})_2(\text{CO})_8]$ with the thermal ellipsoids drawn at the 50% probability level. The hydrogen atoms have been omitted for clarity.

Table 2
Selected distances (Å) and angles (°) for $[\text{Fe}(\mu^2\text{-SiMe}_2)(\text{CO})_4]_2$ and $[\text{Fe}(\mu^2\text{-SiMeCl})(\text{CO})_4]_2$

	$[\text{Fe}_2(\mu^2\text{-SiMe}_2)_2(\text{CO})_8]$			$[\text{Fe}_2(\mu^2\text{-SiMeCl})_2(\text{CO})_8]$		
	Molecule 1		Molecule 2			
Fe–Si	Fe(1)–Si(1A)	2.400(3)	Fe(2)–Si(2)	2.412(3)	Fe(1)–Si(1A)	2.3588(19)
	Fe(1)–Si(1)	2.402(3)	Fe(2)–Si(2B)	2.414(3)	Fe(1)–Si(1)	2.3631(19)
Si···Si	Si(1)–Si(1A)	2.866(5)	Si(2)–Si(2B)	2.900(5)	Si(1)–Si(1A)	2.829(3)
Fe···Fe	Fe(1)–Fe(1A)	3.853(3)	Fe(2)–Fe(2B)	3.858(3)	Fe(1)–Fe(1A)	3.7808(18)
Si–X, X = C or Cl	Si(1)–C(5)	1.894(9)	Si(2)–C(11)	1.882(12)	Si(1)–C(5)	1.919(5)
	Si(1)–C(6)	1.897(10)	Si(2)–C(12)	1.908(12)	Si(1)–Cl(1)	2.094(2)
Fe–Si–Fe	Fe(1A)–Si(1)–Fe(1)	106.72(9)	Fe(2)–Si(2)–Fe(2B)	106.15(11)	Fe(1A)–Si(1)–Fe(1)	106.39(7)
Si–Fe–Si	Si(1A)–Fe(1)–Si(1)	73.28(9)	Si(2)–Fe(2)–Si(2B)	73.85(11)	Si(1A)–Fe(1)–Si(1)	73.61(7)
C–Si–X, X = C or Cl	C(5)–Si(1)–C(6)	101.6(5)	C(11)–Si(2)–C(12)	103.7(6)	C(5)–Si(1)–Cl(1)	101.23(18)
C=O tipping angles	C(2)–Fe(1)–Fe(1A)	83.7(3)	C(9)–Fe(2)–Fe(2B)	82.3(4)	C(4)–Fe(1)–Fe(1A)	84.15(18)
	C(4)–Fe(1)–Fe(1A)	82.5(3)	C(7)–Fe(2)–Fe(2B)	82.6(4)	C(3)–Fe(1)–Fe(1A)	84.53(18)

The structures of other iron–silicon four-membered rings show considerable variability in the iron–silicon distances (2.297–2.421 Å) and in other parameters [4a,22]. Two such rings show Fe–Fe bonds, whereas another shows even shorter Si–Si distances (2.483 Å) than in $[\text{Fe}_2(\mu\text{-SiMe}_2)_2(\text{CO})_8]$ and $[\text{Fe}_2(\mu\text{-SiMeCl})_2(\text{CO})_8]$ [6]. The structures of $[\text{Fe}_2(\mu\text{-SiMe}_2)_2(\text{CO})_8]$ and $[\text{Fe}_2(\mu\text{-SiMeCl})_2(\text{CO})_8]$ are intermediate between the two extremes of iron–silicon four-membered ring structures.

The structures of $[\text{Fe}_2(\mu\text{-SiMe}_2)_2(\text{CO})_8]$ and $[\text{Fe}_2(\mu\text{-SiMeCl})_2(\text{CO})_8]$ show several other notable features. These structures contain relatively short intramolecular C=O···H–C contacts, which are shown in Fig. 3 for $[\text{Fe}_2(\mu\text{-SiMe}_2)_2(\text{CO})_8]$. $[\text{Fe}_2(\mu\text{-SiMeCl})_2(\text{CO})_8]$ shows similar interactions and the distances and angles involved in these short contacts for both rings are listed in Table 3.

Weak C=O···H–C hydrogen bonds formed by terminal carbonyl ligands in iron complexes have O···C distances of 3.4–3.9 Å with H···O=C angles ranging 80–180° [27,28]. Except for a 61° angle in one of the short contacts of $[\text{Fe}_2(\mu\text{-SiMeCl})_2(\text{CO})_8]$, the metrical data in Table 3 do not vary significantly from these ranges. On the other hand, C=O···H–C hydrogen bonds are usually intermolecular rather than intramolecular [27]. The O···H–C interactions may form because C–H groups adjacent to silicon are somewhat acidic [28,29]. However, such interactions could be caused by the forced proximity of the methyl groups to the carbonyl ligands. Forced, intramolecular, hydrogen bonding interactions can be either stabilizing or destabilizing [28]. $[\text{Fe}_2(\mu\text{-SiMe}_2)_2(\text{CO})_8]$ and $[\text{Fe}_2(\mu\text{-SiMeCl})_2(\text{CO})_8]$ are not the only rings to show such intramolecular O···C short contacts. Using the data in the original paper [30], we calculate O···C distances of 2.85–2.93 Å and H···O=C angles of 80–83° for $[\text{Fe}_2(\mu\text{-SnMe}_2)_2(\text{CO})_8]$. We suspect the presence of such intramolecular O···C short contacts may be a general phenomenon.

Another notable feature is that the carbonyl ligands involved in the C=O···H–C contacts are tipped in towards the iron–silicon ring and, thereby, are tipped toward rather than away from the sterically bulkier areas of the two rings. The tipping of carbonyl ligands toward the Group 14 element in mononuclear complexes appears to have been first observed by MacDiarmid in 1970 [31]. In dinuclear M_2E_2 (E = Group 14) rings (see below) the tipping is evidenced by a displacement of the carbonyl ligand toward the M–M vector, which also brings the carbonyl ligand closer to the Group 14 atom. Such tipping occurs even in complexes where no O···H–C interactions appear to be possible [6,21b,32]. Though no general rules have been developed for predicting when such tipping will occur, we note that tipping of carbonyl ligands in Fe_2Si_2 and Fe_2Si rings was not observed when the iron atom was also involved in agostic Si–H–Fe interactions [22b].

Crystals suitable for X-ray crystallography of $[\text{Fe}(\text{SiMe}_2(\text{HMPA}))(\text{CO})_4]$ and $[\text{Fe}(\text{SiMeCl}(\text{HMPA}))(\text{CO})_4]$ were obtained by cooling toluene solutions to –10°C. Several attempts to obtain crystals of $[\text{Fe}(\text{SiMe}_2(\text{DABCO}))(\text{CO})_4]$ were unsuccessful. The crystal structure of $[\text{Fe}(\text{SiMe}_2(\text{HMPA}))(\text{CO})_4]$ had been

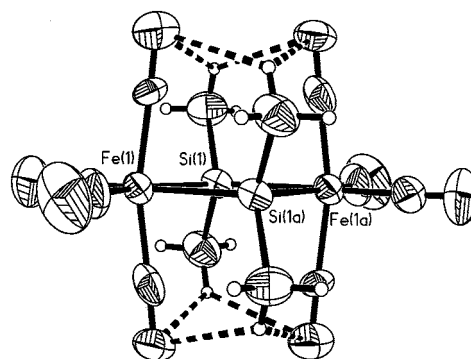


Fig. 3. The O···H–C short contacts for $[\text{Fe}(\text{CO})_4(\text{SiMe}_2)_2]$.

Table 3

The C–H⋯O short contacts for [Fe(μ^2 -SiMe₂)(CO)₄]₂ and [Fe(μ^2 -SiMeCl)(CO)₄]₂ (Å and °)

Compound	C–H⋯O=C	d(C–H)	d(H⋯O)	d(O⋯C)	∠(C–H⋯O)	∠(H⋯O=C)
[Fe(μ^2 -SiMe ₂)(CO) ₄] ₂	C(5)–H(5B)⋯O(2)=C(2)	0.96	2.70	3.395(15)	130.2	80.4
	C(6)–H(6C)⋯O(4)=C(4)	0.96	2.78	3.379(13)	121.6	82.4
	C(11)–H(11C)⋯O(9)=C(9)	0.96	2.76	3.433(16)	127.9	77.6
	C(12)–H(12A)⋯O(7)=C(7)	0.96	2.60	3.357(18)	136.4	79.0
[Fe(μ^2 -SiMeCl)(CO) ₄] ₂	C(5)–H(5B)⋯O(3)=C(3)	0.98	2.82	3.429(7)	120.8	81.9
	C(5)–H(5B)⋯O(4A)=C(4A)	0.98	2.74	3.438(7)	128.6	79.7
	C(5)–H(5A)⋯O(2A)=C(2A)	0.98	3.19	3.830(7)	124.2	60.6

previously reported by Zybill and is identical to that we observed except that we obtained a higher *R*-value [6]. In comparisons of structural data, the parameters obtained by Zybill will be used. The three [Fe(SiMe_{2–n}Cl_n(HMPA))(CO)₄] (*n* = 0, 1 or 2) complexes are isostructural crystallizing in the space group *P*2₁/*n* with two crystallographically independent molecules per unit cell. Consistent with the isostructural nature of the three [Fe(SiMe_{2–n}Cl_n(HMPA))(CO)₄] complexes, the methyl and chloro substituents of [Fe(SiMeCl(HMPA))(CO)₄] were disordered and each molecule was found to be a 67:33 (%) mixture of two conformers. A thermal ellipsoid drawing of one conformer of [Fe(SiMeCl(HMPA))(CO)₄] is shown in Fig. 4. A carbonyl oxygen atom, O(4), was also treated with a disorder model. Selected bond distances and angles for [Fe(SiMeCl(HMPA))(CO)₄] are listed in Table 4.

The structure of [Fe(SiMeCl(HMPA))(CO)₄] is essentially the same to that of other [Fe(SiRR'(HMPA))(CO)₄] complexes with a trigonal bipyramidal geometry at the iron atom and distorted tetrahedral geometries at the silicon and phosphorus atoms. In general, [Fe(SiMeCl(HMPA))(CO)₄] shows structural properties intermediate to those of [Fe(SiMe₂(HMPA))(CO)₄] and [Fe(SiCl₂(HMPA))(CO)₄] or properties that are very similar to theirs. The Fe–Si bond distances for the two molecules of [Fe(SiMeCl(HMPA))(CO)₄] are toward the short end of the range reported for [Fe(SiRR'(HMPA))(CO)₄] complexes (2.214(1)–2.313(1) Å) [3b,c,6,33]. The known range of Fe–Si single bonds (2.20–2.42 Å [1a]) includes bonds that are shorter than those of any [Fe(SiRR'(HMPA))(CO)₄] complex. It has been observed that a higher electron deficiency at the silicon atom of a base-stabilized silylene complex yields shorter metal–silicon and metal–donor bonds [3c]. The three [Fe(SiMe_{2–n}Cl_n(HMPA))(CO)₄] complexes follow this trend. As shown by the sum of the angles at silicon that do not include the oxygen of the HMPA ligand (336–340°), the three [Fe(SiMe_{2–n}Cl_n(HMPA))(CO)₄] complexes exhibit a similar tendency toward planarity at the silicon atom.

Table 5 compares selected bond distances and angles for [Fe₂(μ -SiRR')₂(CO)₈] and [Fe(SiRR'(HMPA))(CO)₄] for the dimethyl and the methyl chloro complexes. This is the first time direct structural comparison between a ring and its counterpart base-stabilized silylene is available. An important structural difference between [Fe₂(μ -SiRR')₂(CO)₈] and [Fe(SiRR'(HMPA))(CO)₄] is the Fe–Si bond distance, which is longer in the ring. This observation is consistent with the idea that the Fe–Si bonds in the base-stabilized silylene complexes have some multiple bond character. The sum of the angles at silicon not including the angles to the base has often been used to judge the silylene character in a base-stabilized metal silylene [3a–c]. Such sums have been calculated for [Fe₂(μ -SiMe₂)₂(CO)₈] and [Fe₂(μ -SiMeCl)₂(CO)₈] by considering one of the iron centers that each silicon atom is bound to as the base. For both rings this sum is very close to the expected value for tetrahedral coordination of 327° and is roughly 13° less than the sum for the analogous base-stabilized silylene complex.

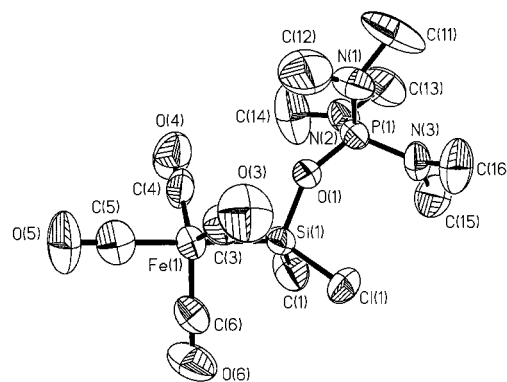


Fig. 4. Molecular structure of one of the conformers of [Fe(SiMeCl(HMPA))(CO)₄] with the thermal ellipsoids drawn at the 50% probability level. Hydrogen atoms have been omitted for clarity.

Table 4
Selected distances (Å) and angles (°) [Fe(SiMeCl(HMPA))(CO)₄]

Molecule 1		Molecule 2	
Fe(1)–C(4)	1.749(6)	Fe(2)–C(8)	1.747(5)
Fe(1)–C(6)	1.753(5)	Fe(2)–C(9)	1.749(6)
Fe(1)–C(3)	1.763(5)	Fe(2)–C(7)	1.751(5)
Fe(1)–C(5)	1.771(5)	Fe(2)–C(10)	1.781(5)
Fe(1)–Si(1)	2.2466(13)	Fe(2)–Si(2)	2.2318(14)
Si(1)–O(1)	1.694(3)	Si(2)–O(2)	1.699(3)
Si(1)–Cl(1')	1.947(15)	Si(2)–C(2)	1.84(3)
Si(1)–C(1)	1.99(2)	Si(2)–C(2')	1.87(4)
Si(1)–Cl(1)	2.004(6)	Si(2)–Cl(2')	2.034(17)
Si(1)–C(1')	2.11(3)	Si(2)–Cl(2)	2.066(8)
C(4)–Fe(1)–C(6)	121.3(2)	C(8)–Fe(2)–C(9)	120.4(2)
C(4)–Fe(1)–C(3)	119.7(2)	C(8)–Fe(2)–C(7)	118.9(2)
C(6)–Fe(1)–C(3)	116.8(2)	C(9)–Fe(2)–C(7)	118.0(2)
C(4)–Fe(1)–C(5)	93.2(2)	C(8)–Fe(2)–C(10)	94.6(2)
C(6)–Fe(1)–C(5)	95.9(2)	C(9)–Fe(2)–C(10)	95.7(2)
C(3)–Fe(1)–C(5)	95.8(2)	C(7)–Fe(2)–C(10)	96.1(2)
C(4)–Fe(1)–Si(1)	84.25(15)	C(8)–Fe(2)–Si(2)	85.11(15)
C(6)–Fe(1)–Si(1)	84.74(15)	C(9)–Fe(2)–Si(2)	84.33(16)
C(3)–Fe(1)–Si(1)	86.15(15)	C(7)–Fe(2)–Si(2)	84.22(14)
C(5)–Fe(1)–Si(1)	177.36(15)	C(10)–Fe(2)–Si(2)	179.67(17)
O(1)–Si(1)–Cl(1')	105.6(7)	O(2)–Si(2)–C(2)	102.7(9)
O(1)–Si(1)–C(1)	99.3(9)	O(2)–Si(2)–C(2')	100.8(15)
Cl(1')–Si(1)–C(1)	7.6(15)	C(2)–Si(2)–C(2')	105.6(19)
O(1)–Si(1)–Cl(1)	104.4(3)	O(2)–Si(2)–Cl(2')	103.6(5)
Cl(1')–Si(1)–Cl(1)	97.6(6)	C(2)–Si(2)–Cl(2')	5.5(16)
C(1)–Si(1)–Cl(1)	103.4(8)	C(2')–Si(2)–Cl(2')	110.6(17)
O(1)–Si(1)–C(1')	96.8(12)	O(2)–Si(2)–Cl(2)	102.4(2)
Cl(1')–Si(1)–C(1')	105.8(14)	C(2)–Si(2)–Cl(2)	97.7(10)
C(1)–Si(1)–C(1')	111.1(14)	C(2')–Si(2)–Cl(2)	8.0(19)
Cl(1)–Si(1)–C(1')	9.8(15)	Cl(2')–Si(2)–Cl(2)	102.6(6)
O(1)–Si(1)–Fe(1)	112.04(10)	O(2)–Si(2)–Fe(2)	112.97(10)
Cl(1')–Si(1)–Fe(1)	118.7(5)	C(2)–Si(2)–Fe(2)	120.9(10)
C(1)–Si(1)–Fe(1)	118.9(7)	C(2')–Si(2)–Fe(2)	111.6(15)
Cl(1)–Si(1)–Fe(1)	116.6(2)	Cl(2')–Si(2)–Fe(2)	116.0(5)
C(1')–Si(1)–Fe(1)	115.3(11)	Cl(2)–Si(2)–Fe(2)	117.4(2)
P(1)–O(1)–Si(1)	150.64(18)	P(2)–O(2)–Si(2)	148.08(17)

3.4. Structural analysis and computational studies *M*₂E₂ rings of type 1

3.4.1. Structural analysis

To put our structural theoretical studies in a wider

context, we have searched in the *Cambridge Structural Database* [20] for all known structures with M₂E₂ rings of type 1, in which M is any transition metal and E any Group 14 element. Some structural parameters for these compounds are collected in Table 6.

To detect the existence of through-ring bonding, and given the variety of M and E atoms, we look at the difference between the M–M and E–E interatomic distances and the corresponding atomic radii [8] sum (Δ_{MM} and Δ_{EE} , respectively, in Table 6). Eighteen crystallographically independent molecules of sixteen compounds with NRE = 20 (i.e. FEC = 8) have been found to present M–M distances across the ring larger than 3.78 Å (i.e. $\Delta_{MM} > 1.1$ Å, Table 6) and E–M–E angles between 73 and 80°. Clearly, no M–M bonding exists in any of these compounds. In contrast, ten complexes with NRE = 18 have M–M distances quite close to the atomic radii sum ($\Delta_{MM} \leq 0.32$ Å) and large E–M–E bond angles (98–110°). The structural differences between compounds with NRE = 20 (FEC = 8) and those with NRE = 18 (FEC = 6) are clear and consistent with the framework electron counting rules.

The E–E distances should be considered non-bonding for all complexes with 18 ring electrons, as indicated by $\Delta_{EE} > 1.3$ Å. Complexes with NRE = 20 in which the bridging atom is C, Si or Ge present shorter E–E distances, if still significantly longer than the atomic radii sum ($\Delta_{EE} > 0.6$ Å) and becomes relatively close to the atomic radii sum for the heavier elements, Sn and Pb ($\Delta_{EE} \approx 0.3$ Å).

In all complexes the E atoms keep a nearly tetrahedral geometry (see R–E–R angles in Table 6), with the exception of [Fe₂(μ-GeC₄H₄Me₂)₂(CO)₈] [36] in which the small C–Ge–C bond angle is imposed by the cyclic nature of the germylene group. In contrast, the bond angles around the transition metal atom are significantly distorted from the octahedral values. Hence, the axial ligands bend toward the center of the molecule, as reflected by M–M–L_{ax} angles between 78 and 86° in complexes with NRE = 20, as found in the structures of [Fe₂(μ-SiMe₂)₂(CO)₈] and [Fe₂(μ-SiMeCl)₂(CO)₈] (see

Table 5
Comparisons among selected bond distances and angles for [Fe(μ²-SiMe₂)(CO)₄]₂, [Fe(μ²-SiMeCl)(CO)₄]₂, [Fe(SiMe₂(HMPA))(CO)₄], [Fe(SiMeCl(HMPA))(CO)₄]

	[Fe(CO) ₄ (SiMe ₂) ₂]	Fe(CO) ₄ (SiMe ₂ (HMPA))	[Fe(CO) ₄ (SiMeCl)] ₂	Fe(CO) ₄ (SiMeCl(HMPA))
Fe–Si (Å)	2.407	2.287	2.36095	2.2392
(avg.)		(avg.)	(avg.)	(avg.)
Si–C (Å)	1.895	1.860	1.919(5)	1.95
(avg.)		(avg.)		(avg.)
Si–Cl (Å)			2.094(2)	2.013
				(avg.)
X–Si–X (°)	102.7	107.9	101.23(18)	104
X = C or Cl	(avg.)	(avg.)		(avg.)
Σ ∠ at Si (°)	326.6	339.4	325.9	338.2
(avg.)	(avg.)	(avg.)	(avg.)	(avg.)

Table 6

Structural data for binuclear complexes of the type $[M_2(\mu-ER_2)_2L_8]$, where E is a Group 14 element and M is any transition metal

Compound	NRE	M–M	Δ_{MM}	E–E	Δ_{EE}	M–E	M–E–M	R–E–R	$L_{eq}ML_{eq}$	MML_{ax}	Ref.	Refcode
$[Fe_2(\mu-SiMe_2)_2(CO)_8]$	20	3.853	1.17	2.866	0.73	2.401	106.7	101.6	104.4	83.1		This work
$[Fe_2(\mu-SiMe_2)_2(CO)_8]$	20	3.858	1.17	2.900	0.76	2.413	106.2	103.7	106.1	82.5		This work
$[Fe_2(\mu-SiMeCl)_2(CO)_8]$	20	3.781	1.10	2.829	0.69	2.361	106.4	101.2	103.4	84.3		This work
$[Fe_2(\mu-GeEt_2)_2(CO)_8]$	20	3.943	1.26	3.049	0.65	2.492	104.6	105.1	96.7	81.0	[34]	FECEGE
$[Fe_2(\mu-GeClCH_2SiMe_2-CH_2Cl)_2(CO)_8]$	20	3.846	1.17	3.000	0.60	2.439	104.1	103.1	100.5	83.6	[35]	BAYMUJ
$[Fe_2(\mu-GeC_4H_4Me_2)_2(CO)_8]$	20	3.929	1.25	3.001	0.60	2.472	105.2	90.0	100.9	80.8	[36]	JEGFAC
$[Os_2(\mu-GeMe_2)_2(CO)_8]$	20	4.105	1.29	3.161	0.76	2.591	104.8	106.2	104.5	82.7	[37]	ZUYBOK
$[Fe_2(\mu-SnMe_2)_2(CO)_8]$	20	4.130	1.45	3.313	0.21	2.647	102.5	108.9	118.5	82.3	[30]	MSNCFE
$[Fe_2(\mu-SnMe_2)_2(CO)_8]$	20	4.139	1.46	3.251	0.15	2.632	103.7	105.2	98.8	77.8		MSNCFE
$[Fe_2(\mu-SnCp)_2(CO)_8]$	20	4.136	1.46	3.347	0.25	2.660	102.0	101.1	99.3	81.9	[38]	CPSNCI
$[Rh_2(\mu-SnCl_2)(SnCl_3)_2(CNAr)_6]$	20	4.164	1.38	3.216	0.12	2.630	104.6	98.7	90.5	88.7	[39]	JKWUV
$[Os_2(\mu-SnMe_2)_2(CO)_8]$	20	4.374	1.55	3.376	0.28	2.763	104.7	106.5	102.0	81.4	[40]	ZUXZUN
$[Os_2(\mu-SnMe_2)_2(CO)_7(PMe_3)]$	20	4.372	1.55	3.390	0.29	2.766	104.4	104.7	100.5	82.0	[41]	TENKEC
$[Os_2(\mu-Sn^tBu)_2(CO)_8]$	20	4.414	1.59	3.487	0.39	2.812	103.4	104.8	96.5	85.7	[41]	TENJUR
$[Fe_2(\mu-PbEt_2)_2(CO)_8]$	20	4.272	1.59	3.408	-0.23	2.732	102.8	106.8	97.9	79.6	[42]	KAVSUV01
$[Os_2(\mu-PbMe_2)_2(CO)_8]$	20	4.423	1.60	3.540	-0.10	2.832	102.7	100.6	96.0	81.0	[41]	TENJOL
$[Os_2(\mu-PbMe_2)_2(CO)_8]$	20	4.436	1.62	3.539	-0.10	2.837	102.8	108.6	98.2	81.0		TENJOL
$[Fe_2(\mu-SnCl\{W(CO)_5\})_2(CO)_8]^{2-}$	20	4.127	1.45	3.445	0.35	2.688	100.3	100.8	101.1	80.6	[43]	SADROE
$[Fe_2(\mu-SnBu)_2(CO)_6(dppm)_2]$	20	4.184	1.50	3.283	0.18	2.659	103.8	107.1	93.9	80.3	[44]	TECHOY
$[Mn_2(\mu-CF_2)_2(CO)_8]$	18	2.664	-0.14	3.076	1.50	2.034	81.8	102.7	95.4	93.2	[45]	DOFPET
$[Mn_2(\mu-SiPh)_2(CO)_8]$	18	2.871	0.07	3.852	1.71	2.402	73.4	109.4	96.4	91.1	[46]	DPSCMN
$[Mn_2(\mu-GeBr\{Mn(CO)_5\})_2(CO)_8]$	18	2.924	-0.21	4.008	1.61	2.481	72.2	101.9	95.2	90.8	[47]	FOMVIM
$[Mn_2(\mu-GeI\{Mn(CO)_5\})_2(CO)_8]$	18	2.932	-0.21	4.039	1.64	2.496	72.0	101.9	95.8	91.0	[48]	FOJDEN
$[Mn_2(\mu-SnCl\{Mn(CO)_5\})_2(CO)_8]$	18	3.091	-0.05	4.241	1.14	2.624	72.2	102.6	94.7	89.3	[49]	FOLJEV
$[Mn_2(\mu-SnBr\{Mn(CO)_5\})_2(CO)_8]$	18	3.085	-0.05	4.254	1.15	2.627	71.9	102.7	94.7	89.5	[50]	FOLJEX
$[Re_2(\mu-SnCl\{Re(CO)_4PPh_3\})_2(CO)_8]$	18	3.160	0.09	4.531	1.43	2.762	69.8	104.9	102.6	88.9	[51]	CIWVOT
$[Re_2(\mu-SnI\{Re(CO)_4PPh_3\})_2(CO)_8]$	18	3.176	0.10	4.546	1.45	2.773	69.9	105.4	94.8	90.0	[52]	CESRIB
$[Ru_2(\mu-SiMe_2)_2(SiMe_3)_2(CO)_6]$	18	2.959	0.02	3.886	1.75	2.442	74.6	105.5	86.4	91.8	[53]	MSICRU
$[Ru_2(\mu-SnMe_2)_2(SnMe_3)_2(CO)_6]$	18	3.116	0.18	4.329	2.19	2.667	71.5	108.5	86.0	90.0	[54]	MSNCRU

discussion under Section 3.3). In compounds with NRE = 18, however, the position of the axial ligands corresponds to practically undistorted octahedra (89–93°). The $L_{eq}M-L_{eq}$ angles are clearly larger than 90° when NRE = 20, and smaller for those having NRE = 18.

3.4.2. Theoretical results

Density functional (DFT) calculations were performed on complexes of formula $[M_2(\mu-ER_2)_2L_8]^{n+}$ corresponding to electron counts NRE = 18 or 20 and the geometry shown in **1**. The atomic coordinates of the optimized geometries are supplied as *Supporting Infor-*

mation. The main bonding parameters for the optimized structures are presented in Table 7.

The DFT results confirm the existence of one minimum with structure **1a** for compounds with NRE = 20. The calculated through-ring distances are slightly longer than the experimental values as a result of the overestimation (by about 0.08 Å) of the M–E bond distances. However, the large Δ_{MM} and Δ_{EE} values as well as the E–M–E angles (73–79° compared to the experimental values of 73–80°) are consistent with the absence of through-ring bonding interaction. Also, the similarity between the calculated structure of $[Fe_2(\mu-SiH_2)_2(CO)_8]$ to the actual structures of $[Fe_2(\mu-$

Table 7
Theoretical parameters for optimized binuclear complexes with general formula $[\text{M}_2(\mu\text{-ER}_2)_2(\text{CO})_8]$

Compounds	Structure	NRE	E_{rel}	$\text{M}\cdots\text{M}$	Δ_{MM}	E–E	Δ_{EE}	M–E	E–M–E	M–E–M	R–E–R	$L_{\text{eq}}\text{M}L_{\text{eq}}$	$\text{MM}L_{\text{ax}}$
$[\text{Mn}_2(\mu\text{-SiH}_2)_2(\text{CO})_8]^{2-}$	1a	20		4.034	1.23	2.987	0.85	2.510	73.0	107.0	101.9	100.5	82.5
$[\text{Fe}_2(\mu\text{-CH}_2)_2(\text{CO})_8]$	1a	20		3.269	0.24	2.641	1.28	2.101	77.9	102.1	108.2	102.3	86.7
$[\text{Fe}_2(\mu\text{-SiH}_2)_2(\text{CO})_8]$	1a	20		3.908	1.23	2.963	0.82	2.452	74.3	105.7	107.0	101.6	83.3
$[\text{Fe}_2(\mu\text{-GeH}_2)_2(\text{CO})_8]$	1a	20		3.973	0.95	3.090	0.75	2.517	75.7	104.3	107.1	101.3	82.5
$[\text{Fe}_2(\mu\text{-SnH}_2)_2(\text{CO})_8]$	1a	20		4.167	1.15	3.342	0.42	2.672	77.4	102.6	108.4	100.6	81.4
$[\text{Fe}_2(\mu\text{-PbH}_2)_2(\text{CO})_8]$	1a	20		4.236	1.22	3.470	0.39	2.738	78.6	101.4	108.5	100.0	80.8
$[\text{Fe}_2(\mu\text{-SiMe}_2)_2(\text{CO})_8]$	1a	20		3.910	1.23	3.082	0.74	2.489	76.5	103.5	104.5	101.6	83.0
$[\text{Fe}_2(\mu\text{-SiMeCl})_2(\text{CO})_8]$	1a	20		3.849	1.17	3.004	0.86	2.441	75.9	104.1	100.3	100.0	84.8
$[\text{Ru}_2(\mu\text{-SiH}_2)_2(\text{CO})_8]$	1a	20		4.126	1.19	3.085	0.95	2.576	73.6	106.4	106.4	102.0	83.5
$[\text{Os}_2(\mu\text{-SiH}_2)_2(\text{CO})_8]$	1a	20		4.147	1.33	3.145	1.01	2.602	74.3	105.7	106.2	101.3	85.5
$[\text{Mn}_2(\mu\text{-SiH}_2)_2(\text{CO})_8]$	1b	18	36.4	4.614	1.81	2.362	0.22	2.592	54.2	125.8	119.2	95.8	87.4
$[\text{Mn}_2(\mu\text{-SiH}_2)_2(\text{CO})_8]$	1c	18	0	2.956	0.16	3.828	1.69	2.418	104.6	75.4	106.4	95.8	90.4
$[\text{Fe}_2(\mu\text{-CH}_2)_2(\text{CO})_8]^{2+}$	1b	18	31.1	4.181	1.16	1.473	0.11	2.216	38.8	141.2	115.9	97.7	90.2
$[\text{Fe}_2(\mu\text{-SiH}_2)_2(\text{CO})_8]^{2+}$	1c	18	0	2.597	-0.42	3.137	1.78	2.036	100.8	79.2	110.1	95.5	93.5
$[\text{Fe}_2(\mu\text{-CH}_2)_2(\text{CO})_8]^{2+}$	1b	18	22.1	4.613	1.93	2.384	0.24	2.596	54.7	125.3	121.6	95.3	88.1
$[\text{Fe}_2(\mu\text{-SiH}_2)_2(\text{CO})_8]^{2+}$	1c	18	0	2.937	0.26	3.867	1.73	2.428	105.6	74.4	110.8	95.3	91.1
$[\text{Fe}_2(\mu\text{-SnH}_2)_2(\text{CO})_8]^{2+}$	1b	18	31.3	4.846	1.83	2.891	-0.03	2.821	61.6	118.4	125.7	94.1	86.3
$[\text{Fe}_2(\mu\text{-SnH}_2)_2(\text{CO})_8]^{2+}$	1c	18	0	3.172	0.15	4.324	1.40	2.681	107.5	72.5	115.4	95.0	88.9

$\text{SiMe}_2)_2(\text{CO})_8]$ and $[\text{Fe}_2(\mu\text{-SiMeCl})_2(\text{CO})_8]$ indicates that the C–H \cdots O \equiv C short contacts observed in the latter two are not significant in determining the overall structure because such contacts cannot exist in $[\text{Fe}_2(\mu\text{-SiH}_2)_2(\text{CO})_8]$. The presence of a chlorine atom bonded to silicon results in a ring contraction as seen in Fe–Si bond distances some 0.05 Å shorter, in agreement with the behavior already discussed for experimental structures with Fe_2Si_2 or Fe_2Ge_2 cores (Table 6). No significant differences can be found as a result of metal atom substitution.

The two-electron oxidation of the above complexes gives compounds with two energy minima displaying short E–E ($\Delta_{\text{EE}} < 0.26$ Å, **1b**) or M–M ($\Delta_{\text{MM}} < 0.24$ Å, **1c**) distances, respectively, in agreement with the qualitative predictions for NRE = 18 and FEC = 6 [8]. For the cases analyzed, the metal–metal bonded isomer (**1c**) is clearly predicted to be more stable than the bridge–bridge bonded one. Experimental data are in agreement with this finding, because all the 18-electron complexes in this family present a short M–M distance (Table 6). Besides ring squeezing, characteristic of structures **1b** and **1c**, the main structural differences found upon decreasing the NRE in our model complexes from 20 to 18 are: (1) the M–E distances suffer a significant increase for **1b** but are practically unaffected in **1c**; (2) an increase in the R–E–R bond angles, which is more pronounced for structure **1b**; (3) a decrease in $L_{\text{eq}}\text{M}L_{\text{eq}}$ bond angles, and (4) an increase in the $\text{M}L_{\text{ax}}$ bond angles, more pronounced for structure **1c**. Except for the changes in the M–E distances, for which there is no comparable experimental data, all these trends are consistent with the experimental data discussed above.

Two structural effects are observed from the theoretical structures of the 20-electron Fe complexes. First, one can see that the $\text{M}L_{\text{ax}}$ angles adopt values close to 87° (less than 86° experimentally) for compounds with NRE = 20 and values around 91° (89–93° experimentally) for complexes with NRE = 18. If we concentrate on the 20-electron complexes, we can see that such angle decreases with increasing M–M distance (Fig. 5), a correlation that is also found for the experimental data.

Iron complexes with 18 ring electrons and short Fe–Fe distances also fit nicely into this correlation. Although there are no experimental iron complexes with 18 ring electrons, the structurally characterized Mn and Ru analogues are also in excellent agreement with the theoretical correlation (Table 7, not shown in Fig. 5 for simplicity). These results are consistent with general rules deduced for analogous molecules with more electronegative bridging atoms [8] and suggest that in the presently studied carbonyl complexes there is an electronic preference for bending the axial bonds inwards, which is sterically prevented as the two metal

atoms approach each other. We note that in all *cis*-Fe(CO)₄L₂ fragments retrieved in a CSD search (21 structures, see Experimental section for details), the two axial carbonyl ligands are bent toward the non-carbonyl ligands. If we define the centroid between the two L's as c, the c–M–CO_{ax} angles equivalent to the M–M–L_{ax} one studied here present values between 80.8 and 87.4°. We therefore conclude that bending of the axial carbonyls is due to the *cis* influence of the equatorial carbonyls that affect d orbital hybridization in the axial direction [55].

A second structural effect concerns the L_{eq}–M–L_{eq} bond angle associated with the terminal equatorial ligands. This angle is calculated to be 100–102° in complexes with NRE = 20 but decreases to 95° for NRE = 18 ones. Even within the set of 20-electron complexes, the L_{eq}–M–L_{eq} angle is seen to increase upon decreasing the E–M–E bond angle (Fig. 6, empty circles).

That such correlation is a typical behavior of the equatorial ligands in an octahedral complex can be seen in the experimental data for all *cis*-Fe(CO)₄L₂ groups found in a structural database analysis, provided no direct L–L bond exists (Fig. 6, solid triangles). A similar trend has been detected for analogous complexes with square planar metal atoms having bidentate terminal ligands [56].

An elegant way to summarize changes in structural parameters consists in using the continuous symmetry measures [57,58]. In brief, the octahedral symmetry measure (or octahedrity) of the coordination sphere of a ML₆ fragment, *S*(O_h), should be zero for a perfect octahedron and increase as any structural parameter is distorted. For the calculated structures with NRE = 20, the octahedrity is progressively lost (i.e. *S*(O_h) becomes larger) as the Fe–Fe distance decreases (Fig. 7, empty circles).

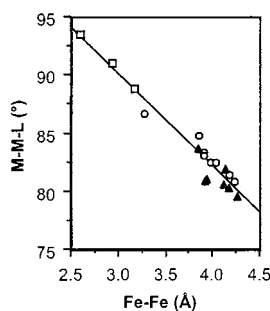


Fig. 5. M–M–L_{axial} angle in [Fe₂(μ-EH₂)₂(CO)₈] complexes as a function of the through-ring M–M distance. Calculated data (Table 1) for molecules with 20 and 18 ring electrons represented by empty circles and squares, respectively. Experimental data for 20-electron complexes (Table 2) represented by closed triangles. The line shown corresponds to a least-squares fitting of calculated and experimental data.

Because we have seen above that the Fe–Fe distance and the M–M–L_{ax} angle are correlated, it is clear that the loss of octahedrity is mostly due to the angular distortion of the axial ligands at long metal–metal distances. This trend is also found in the experimental structural data (Fig. 7, closed circles). In the metal–metal bonded complexes with NRE = 18, *S*(O_h) also increases with the distance, but the susceptibility to this bonding parameter is much larger (Fig. 7, empty and closed triangles for calculated and experimental structures, respectively). This is due to the fact that in such geometry the longer distances correspond to larger atomic size of the bridge (E = C, Si, Sn in our calculations), and the E–M–E bond angle is also larger to allow for a short metal–metal distance. Hence, in compounds with 18 ring electrons and structure **1c**, *S*(O_h) increases with the M–M distance because of the simultaneous distortion from octahedral symmetry of both the M–M–L_{ax} and E–M–E angles.

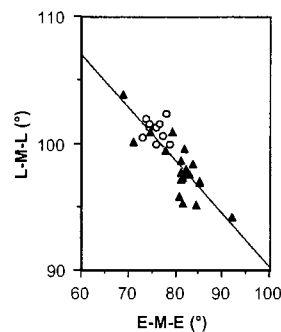


Fig. 6. Bond angle associated to the equatorial terminal ligands as a function of the bridging angle E–M–E in calculated structures of [Fe₂(μ-ER₂)₂(CO)₈] molecules with 20 ring electrons (empty circles). Experimental data for [M₂(μ-ER₂)₂(CO)₈] complexes represented by closed triangles. The line shown corresponds to a least-squares fitting of calculated and experimental data.

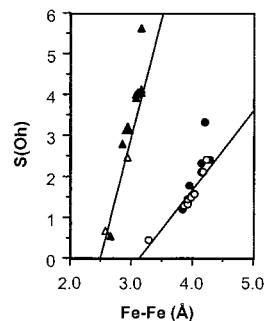


Fig. 7. Octahedrity of the Fe coordination sphere as a function of the Fe–Fe distance in [Fe₂(μ-ER₂)₂(CO)₈] complexes with 20 (empty and closed circles for calculated and experimental data, respectively) and with 18 (empty and closed triangles for calculated and experimental data, respectively) ring electrons. The straight lines shown were obtained by least-squares fitting of the corresponding calculated data.

4. Conclusions

The reactions of the rings $[\text{Fe}_2(\mu\text{-SiMe}_2)_2(\text{CO})_8]$ and $[\text{Fe}_2(\mu\text{-SiMeCl})_2(\text{CO})_8]$ with bases resulted in the destruction of the rings and, in some cases, base-stabilized silylenes were isolated. Structural characterization of these rings showed planar rings, relatively short Si···Si cross ring distances, and C–H···O≡C short contacts. The first direct structural comparisons between metal–silicon four-membered rings and their counterpart base-stabilized silylene complexes were described.

The combined use of theoretical studies and structural database analysis has confirmed that the $[\text{M}_2(\mu\text{-ER}_2)_2(\text{CO})_8]$ compounds follow the framework electron counting rules. Hence, $[\text{Fe}_2(\mu\text{-SiMe}_2)_2(\text{CO})_8]$ and $[\text{Fe}_2(\mu\text{-SiMeCl})_2(\text{CO})_8]$ present 20 ring electrons, or eight framework electrons. The Si–Si distance in such compounds (2.8–2.9 Å exp., 3.0 Å calc.) must be considered as non-bonding, given all the theoretical and structural evidence for isoelectronic compounds. In platinum complexes with a through-ring Si–Si bond, the corresponding distance is ~ 2.6 Å [10]. Two-electron oxidation of such compounds, however, is predicted to yield two isomeric structures: the most stable one, **1c**, would have a short Fe–Fe through-ring distance, but another relative minimum in the potential energy surface is found for geometry **1b** with a short Si–Si distance (~ 2.4 Å). The C–H···O≡C short contacts in the structures of $[\text{Fe}_2(\mu\text{-SiMe}_2)_2(\text{CO})_8]$ and $[\text{Fe}_2(\mu\text{-SiMeCl})_2(\text{CO})_8]$ do not perturb the structure of the ring relative to that of $[\text{Fe}_2(\mu\text{-SiH}_2)_2(\text{CO})_8]$.

5. Supplementary material

Crystallographic data for the structural analyses of $[\text{Fe}_2(\mu\text{-SiMe}_2)_2(\text{CO})_8]$, $[\text{Fe}_2(\mu\text{-SiMeCl})_2(\text{CO})_8]$, $[\text{Fe}(\text{SiMeCl}(\text{HMPA}))(\text{CO})_4]$, and $\text{Fe}(\text{PMe}_3)_2(\text{CO})_3$ have been deposited with the Cambridge Crystallographic Data Centre, CCDC Nos. 151043, 151041, 151042, 151122, respectively. Copies of this information may be obtained free of charge from The Director, CCDC, 12 Union Road, Cambridge CB2 1EZ, UK (fax: +44-1223-336033; e-mail: deposit@ccdc.cam.ac.uk or www: <http://www.ccdc.cam.ac.uk>).

Tables containing atomic coordinates for non-hydrogen atoms, isotropic thermal parameters, bond lengths, bond angles, anisotropic thermal parameters, and positional parameters for hydrogen atoms and some figures for $[\text{Fe}_2(\mu\text{-SiMe}_2)_2(\text{CO})_8]$, $[\text{Fe}_2(\mu\text{-SiMeCl})_2(\text{CO})_8]$, $[\text{Fe}(\text{SiMe}_2(\text{HMPA}))(\text{CO})_4]$, $[\text{Fe}(\text{SiMeCl}(\text{HMPA}))(\text{CO})_4]$ $\text{Fe}(\text{PMe}_3)_2(\text{CO})_3$ are listed. Also tables of atomic coordinates for all optimized structures corresponding to energy minima reported in Table 7 are provided.

Acknowledgements

This material is based upon work supported by the National Science Foundation under Grants No. 9708181 and a grant from the National Science Foundation Chemical Instrumentation Program (CHE-8820644). The support of this research by the University of Akron is gratefully acknowledged. Mass spectral determinations were made at the Midwest Center for Mass Spectroscopy with partial support from National Science Foundation, Biology Division (DIR9017262). C.T. and W.Y. thank Francois Diederich and Peter Chen for hosting sabbatical leaves at ETH-Zürich during which time part of this paper was written. Financial support to this work was also provided by the Dirección General de Enseñanza Superior (DGES) through grant PB98-1166-C02-01 and by Comissionat per a Universitats i Recerca (Generalitat de Catalunya) through grant 1999SGR-0046. The computing resources at the Centre de Supercomputació de Catalunya (CESCA) and at the Centre de Paral·lelisme de Barcelona (CEPBA) were made available in part through grants from Centre Interdepartamental per a la Recerca i la Innovació Tecnològica (CIRIT) and Universitat de Barcelona.

References

- [1] (a) J.Y. Corey, J. Braddock-Wilking, *Chem. Rev.* 99 (1999) 175; (b) M.S. Eisen, Transition-metal silyl complexes, in: Z. Rappoport, Y. Apeloig (Eds.), *The Chemistry of Organic Silicon Compounds*, Part 3, vol. 2, Wiley, New York, 1998 (chap. 35).
- [2] H. Ogino, H. Tobita, *Adv. Organomet. Chem.* 42 (1998) 223.
- [3] (a) P.D. Lickiss, *Chem. Soc. Rev.* 21 (1992) 271; (b) C. Zybilla, *Top. Curr. Chem.* 160 (1991) 1; (c) C. Zybilla, H. Handwerker, H. Friedrich, *Adv. Organomet. Chem.* 36 (1994) 229; (d) R.J.P. Corriu, B.P.S. Chauhan, G.F. Lanneau, *Organometallics* 14 (1995) 1646.
- [4] (a) K.M. Horng, S.L. Wang, C.S. Liu, *Organometallics* 10 (1991) 631; (b) R.J.P. Corriu, G.F. Lanneau, B.P.S. Chauhan, *Organometallics* 12 (1993) 2001; (c) B.P.S. Chauhan, R.J.P. Corriu, G.F. Lanneau, C. Priou, *Organometallics* 14 (1995) 1657.
- [5] (a) K. Ueno, N. Hamashima, H. Ogino, *Organometallics* 11 (1992) 1435; (b) B.K. Campion, R.H. Heyn, T.D. Tilley, *Organometallics* 11 (1992) 3918.
- [6] C. Zybilla, D.L. Wilkinson, C. Leis, H. Handwerker, *Organometallics* 11 (1992) 514.
- [7] (a) K.H. Pannell, H. Sharma, *Organometallics* 10 (1991) 954; (b) K. Ueno, N. Hamashima, M. Shimoi, H. Ogino, *Organometallics* 10 (1991) 959.
- [8] A.A. Palacios, G. Aullón, P. Alemany, S. Alvarez, *Inorg. Chem.* 39 (2000) 3166.
- [9] (a) P. Alemany, S. Alvarez, *Inorg. Chem.* 31 (1992) 4266; (b) G. Aullón, P. Alemany, S. Alvarez, *J. Organomet. Chem.* 478 (1994) 75; (c) S. Alvarez, A.A. Palacios, G. Aullón, *Coord. Chem. Rev.* 185–186 (1999) 431.

- [10] (a) E.A. Zarate, C.A. Tessier-Youngs, W.J. Youngs, *J. Am. Chem. Soc.* 110 (1988) 4068;
(b) E.A. Zarate, C.A. Tessier-Youngs, W.J. Youngs, *J. Chem. Soc. Chem. Commun.* (1989) 577;
(c) L.M. Sanow, M. Chai, D.B. McConnville, K.J. Galat, R.S. Simons, P.L. Rinaldi, W.J. Youngs, C.A. Tessier, *Organometallics* 19 (2000) 192.
- [11] (a) M. Hamidi, A. Lledós, G. Aullón, S. Alvarez, in preparation;
(b) A.B. Anderson, P. Shiller, E.A. Zarate, C.A. Tessier-Youngs, W.J. Youngs, *Organometallics* 8 (1989) 2320.
- [12] D.F. Shriver, M.A. Drezdon, *The Manipulations of Air-Sensitive Compounds*, Wiley, New York, 1986.
- [13] G. Schmid, E. Welz, *Z. Naturforsch. B* 34 (1979) 929.
- [14] (a) E. Carberry, R. West, *J. Am. Chem. Soc.* 91 (1969) 5440;
(b) E. Carberry, R. West, G.E. Glass, *J. Am. Chem. Soc.* 91 (1969) 5446.
- [15] (a) M.J. Therien, W.C. Troglor, *Inorg. Synth.* 25 (1989) 151;
(b) G. BellaChioma, G. Cardaci, A. Macchioni, G. Reichenbach, *J. Organomet. Chem.* 391 (1990) 367.
- [16] M.J. Frisch, G.W. Trucks, H.B. Schlegel, P.M.W. Gill, B.G. Johnson, M.A. Robb, J.R. Cheeseman, T.A. Keith, G.A. Petersson, J.A. Montgomery, K. Raghavachari, M.A. Al-Laham, V.G. Zakrzewski, J.V. Ortiz, J.B. Foresman, J. Cioslowski, B.B. Stefanov, A. Nanayakkara, M. Challacombe, C.Y. Peng, P.Y. Ayala, W. Chen, M.W. Wong, J.L. Andrés, E.S. Replogle, R. Gomperts, R.L. Martin, D.J. Fox, J.S. Binkley, D.J. Defrees, J.P. Baker, J.P. Stewart, M. Head-Gordon, C. Gonzalez, J.A. Pople, gaussian 94 (Revision E.1) Gaussian Inc., Pittsburgh, PA, USA, 1995.
- [17] A.D. Becke, *J. Chem. Phys.* 98 (1993) 5648.
- [18] C. Lee, W. Yang, R.G. Parr, *Phys. Rev. B* 37 (1988) 785.
- [19] (a) W.R. Wadt, P.J. Hay, *J. Chem. Phys.* 82 (1985) 284;
(b) P.J. Hay, W.R. Wadt, *J. Chem. Phys.* 82 (1985) 299.
- [20] F.H. Allen, O. Kennard, *Chem. Des. Autom. News* 8 (1993) 31.
- [21] (a) R.J.P. Corriu, J.J.E. Moreau, *J. Chem. Soc. Chem. Commun.* (1980) 278;
(b) F.H. Carré, J.J.E. Moreau, *Inorg. Chem.* 21 (1982) 3099.
- [22] (a) N.I. Kirillova, A.I. Gusev, O.N. Kalinina, O.B. Afanasova, E.A. Chernyshev, *Metalloorg. Khim.* 4 (1991) 773;
(b) R.S. Simons, C.A. Tessier, *Organometallics* 15 (1996) 2604.
- [23] B.J. Aylett, *Prog. Inorg. Radiochem.* 25 (1982) 1.
- [24] N. Wiberg, H. Schuster, A. Simon, K. Peters, *Angew. Chem. Int. Ed. Engl.* 25 (1986) 79.
- [25] J.E. Huheey, E.A. Keiter, R.L. Keiter, *Inorganic Chemistry*, 4th ed., Harper Collins, New York, 1993 p292.
- [26] H. Nakatsuji, M. Hada, K. Kondo, *Chem. Phys. Lett.* 196 (1992) 404.
- [27] (a) D. Braga, F. Grepioni, K. Birahda, V.R. Pedireddi, G. Desiraju, *J. Am. Chem. Soc.* 117 (1995) 3155;
(b) D. Braga, F. Grepioni, G.J. Desiraju, *Organomet. Chem.* 548 (1997) 33;
(c) D. Braga, F. Grepioni, *Acc. Chem. Res.* 27 (1994) 51;
(d) D. Braga, F. Grepioni, G. Desiraju, *Chem. Rev.* 97 (1997) 1375.
- [28] G.R. Desiraju, T. Steiner, *The Weak Hydrogen Bond*, Oxford University, New York, 1999.
- [29] A.R. Bassindale, S.J. Glynn, P.G. Taylor, Reaction mechanisms of nucleophilic attack at silicon, in: S. Patai, Y. Apeloig (Eds.), *The Chemistry of Organic Silicon Compounds*, vol. 2, Wiley, New York, 1998 (chap. 7).
- [30] C.J. Gilmore, P. Woodward, *J. Chem. Soc. Dalton Trans.* (1972) 1387.
- [31] A.D. Berry, E.R. Corey, A.P. Hagen, A.G. MacDiarmid, F.E. Saalfeld, B.B. Wayland, *J. Am. Chem. Soc.* 92 (1970) 1940.
- [32] (a) S. Li, D.L. Johnson, J.A. Gladysz, K.L. Servis, *J. Organomet. Chem.* 166 (1979) 317;
(b) L. Vancea, M.J. Bennett, C.E. Jones, R.A. Smith, W.A.G. Graham, *Inorg. Chem.* 16 (1977) 897;
(c) R.K. Pomeroy, L. Vancea, H.P. Calhoun, W.A.G. Graham, *Inorg. Chem.* 16 (1977) 1508;
(d) R. Ball, M.J. Bennett, *Inorg. Chem.* 11 (1972) 1806;
(e) M.C. Couldwell, J. Simpson, *J. Chem. Soc. Dalton Trans.* (1976) 714;
(f) J. Silvestre, T.A. Albright, *Isr. J. Chem.* 23 (1983) 139;
(g) S. Alvarez, M. Ferrer, R. Reina, O. Rossell, M. Seco, X. Solans, *J. Organomet. Chem.* 377 (1989) 291;
(h) M.M. Crozat, S.F. Watkins, *J. Chem. Soc. Dalton Trans.* (1972) 2512;
(i) A.G. Berry, E.R. Corey, A.P. Hagen, A.G. MacDiarmid, F.E. Saalfeld, B.B. Wayland, *J. Am. Chem. Soc.* 92 (1970) 1940;
(j) G. Cerveau, F. Carré, R.J.P. Colomer, C.J. Young, L. Ricard, R. Weiss, *J. Organomet. Chem.* 179 (1979) 215;
(k) P.R. Jansen, A. Oskam, K. Olie, *Cryst. Struct. Commun.* 4 (1975) 667;
(l) B.K. Nicholson, W.T. Robinson, J. Simpson, *J. Organomet. Chem.* 47 (1973) 403.
- [33] M.E. Lee, J.S. Han, C.H. Kim, *Bull. Korean Chem. Soc.* 15 (1994) 335.
- [34] J.-C. Zimmer, M. Huber, *C.R. Acad. Sci. Ser. C* 267 (1968) 1685.
- [35] A.L. Bikovets, O.V. Kuz'min, V.M. Vdovin, A. Ya, Sideridu, G.G. Aleksandrov, Yu.T. Struchkov, *Izv. Akad. Nauk. SSSR Ser. Khim.* (1981) 490.
- [36] D. Lei, M.J. Hampden-Smith, E.N. Duesler, J.C. Huffman, *Inorg. Chem.* 29 (1990) 795.
- [37] W.K. Leong, F.W.B. Einstein, R.K. Pomeroy, *Organometallics* 15 (1996) 1589.
- [38] P.G. Harrison, T.J. King, J.A. Richards, *J. Chem. Soc. Dalton Trans.* (1975) 2097.
- [39] S.G. Bott, J.C. Machell, D.M.P. Mingos, M.J. Watson, *J. Chem. Soc. Dalton Trans.* (1991) 859.
- [40] W.K. Leong, F.W.B. Einstein, R.K. Pomeroy, *Organometallics* 15 (1996) 1582.
- [41] W.K. Leong, W.B. Einstein, F.R.K. Pomeroy, *J. Cluster Sci.* 7 (1996) 121.
- [42] M. Heberhold, V. Trobs, W. Milius, B. Wrackmeyer, *Z. Naturforsch. Teil B* 49 (1994) 1781.
- [43] A.L. Balch, M.M. Olmstead, D.P. Oram, *Inorg. Chem.* 27 (1988) 4309.
- [44] P. Braunstein, C. Charles, R.D. Adams, R. Layland, *J. Cluster Sci.* 7 (1996) 145.
- [45] W. Schulze, H. Hartl, K. Seppelt, *Angew. Chem. Int. Ed. Engl.* 25 (1986) 185.
- [46] G.L. Simon, L.F. Dahl, *J. Am. Chem. Soc.* 95 (1973) 783.
- [47] H. Preut, H.-J. Haupt, *Acta Crystallogr. Sect. B* 35 (1979) 729.
- [48] H. Preut, H.-J. Haupt, *Acta Crystallogr. Sect. B* 36 (1980) 678.
- [49] H.-J. Haupt, H. Preut, W. Wolfes, *Z. Anorg. Allgem. Chem.* 446 (1978) 105.
- [50] H. Preut, H.-J. Haupt, *Z. Anorg. Allgem. Chem.* 422 (1976) 47.
- [51] H.-J. Haupt, P. Balsaa, B. Schwab, U. Flörke, H. Preut, *Z. Anorg. Allgem. Chem.* 513 (1984) 22.
- [52] H. Preut, H.-J. Haupt, U. Flörke, *Acta Crystallogr. Sect. C (Cryst. Struct. Commun.)* 40 (1984) 600.
- [53] M.M. Crozat, S.F. Watkins, *J. Chem. Soc. Dalton Trans.* (1972) 2512.
- [54] S.F. Watkins, *J. Chem. Soc. A*, (1969) 1552.
- [55] G. Aullón, S. Alvarez, *Chem. Eur. J* 3 (1997) 655.
- [56] G. Aullón, S. Alvarez, unpublished results.
- [57] M. Pinsky, D. Avnir, *Inorg. Chem.* 37 (1998) 5575.
- [58] H. Zabrodsky, S. Peleg, D. Avnir, *J. Am. Chem. Soc.* 114 (1992) 7843.